JACS
JOURNAL OF THE AMERICAN CHEMICAL SOCIETY
Article
pubs.acs.org/JACS

Synthesis, Molecular Packing, and Thin Film Transistors of Dibenzo[*a*,*m*]rubicenes

Xiao Gu, Xiaomin Xu, Huiyan Li, Zhifeng Liu, and Qian Miao*

Department of Chemistry, The Chinese University of Hong Kong, Shatin, New Territories, Hong Kong, China

Supporting Information

ABSTRACT: We herein report an efficient synthesis of dibenzo[*a*,*m*]rubicene, a new member of nonplanar cyclopenta-fused polycyclic aromatic hydrocarbon, and its derivatives. It is found that the conformation and molecular packing of dibenzo[*a*,*m*]rubicenes in the solid state can be tuned by the substituting groups, and the silylethynylated derivatives of dibenzo[*a*,*m*]rubicenes function as p-type organic semiconductors in solution-processed thin film transistors with field effect mobility of up to 1.0 $cm^2 V^{-1} s^{-1}$.

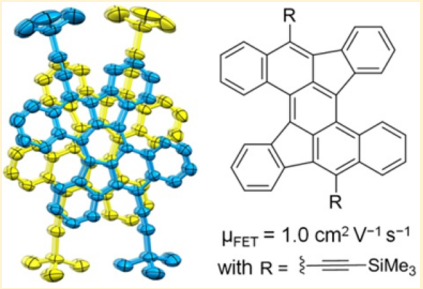

INTRODUCTION

This study explores dibenzo[*a*,*m*]rubicene (**1a** in Figure 1a), a new member of cyclopenta-fused polycyclic aromatic hydrocarbons (CP-PAHs).[1] Dibenzo[*a*,*m*]rubicene was not documented, although its 3,12-*tert*-butyl-substituted derivatives were reported in 2009.[2] Dibenzo[*a*,*m*]rubicene can be regarded as a fragment of C_{70} and formally results from fusing two benzene rings to rubicene (Figure 1b), a planar CP-PAH discovered in the 1920s[3] and recently reported as a p-type semiconductor in organic thin film transistors (OTFTs).[4,5] Unlike rubicene, **1a** is out of plane because of overcrowding in the two fjord regions and thus can be regarded as an analogue of double helicenes.[6] The angularly fused pentacyclic moiety in **1a** as shown with bold lines in Figure 1a is similar to [5]helicene (Figure 1b) but involves less steric hindrance because it has a cyclopentadiene ring replacing a benzene ring in [5]helicene.[7]

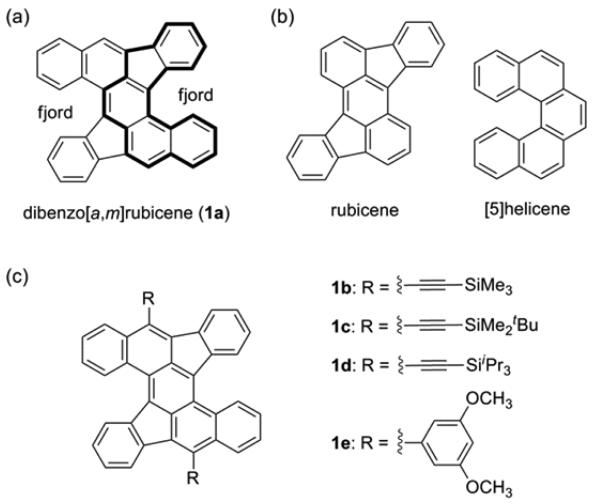

Figure 1. Structures of dibenzo[*a*,*m*]rubicene (**1a**) and related molecules. (a) **1a** with the angularly fused pentacyclic moiety highlighted; (b) rubicene and [5]helicene; (c) new derivatives of **1a**.

Here we report an efficient synthesis of **1a** and its new derivatives and demonstrate that the conformation and molecular packing of dibenzo[*a*,*m*]rubicenes in the solid state can be tuned by the substituting groups. It is found that silylethynylated derivatives **1b** and **1c** function as p-type organic semiconductors in solution-processed OTFTs with field effect mobility of up to 1.0 $cm^2 V^{-1} s^{-1}$.

RESULTS AND DISCUSSION

Synthesis. Shown in Scheme 1 is the synthesis of dibromodibenzo[*a*,*m*]rubicene **2** starting from terephthalate **3**, which was prepared from condensation between dimethyl

Scheme 1. Synthesis of 2

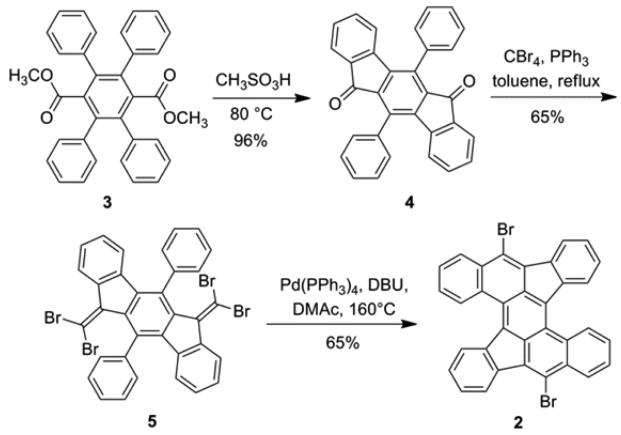

Received: October 13, 2015
Published: December 11, 2015

DOI: 10.1021/jacs.5b10687
J. Am. Chem. Soc. 2015, 137, 16203−16208

acetonedicarboxylate and benzil[8] and the subsequent Diels–Alder reaction with diphenylacetylene by modification of the reported method.[9] Heating **3** with methanesulfonic acid resulted in diketone **4**, which, as reported earlier, was prepared from diethyl 2,3,5,6-tetraphenylterephthalate in two steps (hydrolysis followed by cyclization).[9] The two carbonyl groups of **4** reacted with CBr_4 in the Corey–Fuchs reaction,[10] yielding **5**, which cyclized in an intramolecular Heck-type reaction to give **2**. It was necessary to have this intramolecular Heck-type reaction completed within 15 min. Otherwise, prolonged heating led to debromination of **2**.

Starting from **2**, unsubstituted and functionalized dibenzo[*a*,*m*]rubicenes were easily synthesized, as shown in Scheme 2.

Scheme 2. Synthesis of 1a–e

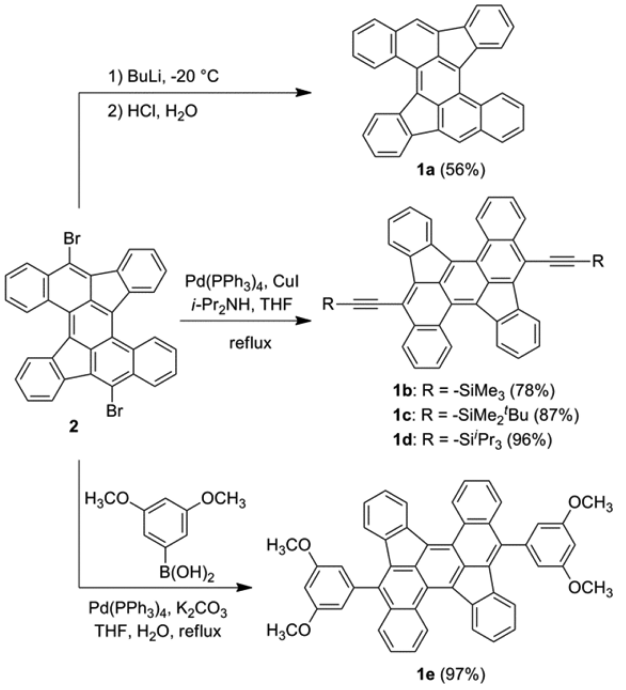

Lithium–halogen exchange on **2** followed by treatment with dilute acid led to **1a**, and the Sonogashira and Suzuki coupling reactions of **2** resulted in **1b–d** and **1e**, respectively. Silyl groups of different sizes are introduced in **1b–d** to tune the packing motifs of dibenzo[*a*,*m*]rubicenes, as inspired by Anthony's silylethynylated pentacenes.[11] Cyclization on the positions *ortho* and *para* to the methoxyl groups of **1e** in a Scholl-type reaction[12] can, in principle, result in aromatic bowls. However, attempted oxidative cyclodehydrogenation of **1e** with $FeCl_3$ or DDQ–methanesulfonic acid did not lead to cyclization.

Conformations. As an analogue of double helicenes, dibenzo[*a*,*m*]rubicene can, in principle, adopt two stable conformations, namely, twisted or *anti*-folded, depending on the helicity of the two fjord regions. To find what kind of conformation **1a–e** adopt at room temperature, molecular structures of **1a–e** were calculated at the B3LYP/6-31G(d,p) level of density functional theory (DFT).[13] As summarized in Table S2 in the Supporting Information, it is found that the twisted conformers of **1a–e** are all thermodynamically more stable than the corresponding *anti*-folded conformers by 12.8 to 14.6 kJ mol^{-1}, which corresponds to equilibrium constants in the range of 175 to 361 at 25 °C for the *anti*-to-twisted isomerization. Moreover, the twisted-to-*anti* interconversion of **1a** occurs through a partially planar transition state (TS), as shown in Figure 2. The energy barrier between twisted-**1a** and

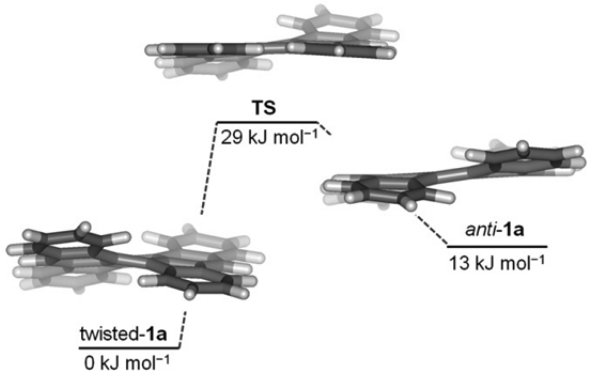

Figure 2. Molecular models of twisted-**1a** and *anti*-**1a** and the transition state as optimized at the B3LYP/6-31G(d,p) level of DFT.

the transition state is calculated as 29 kJ mol^{-1}, which corresponds to a large rate constant (5.2×10^7 s^{-1}) at room temperature (298.15 K), as estimated using the Eyring equation

$$k = \kappa(k_B T/h)\exp(-\Delta G^{\ddagger}/RT)$$

and assuming a value of unity for the transmission coefficient (κ).[14] These calculations indicate that the dominating conformer of **1a–e** is the twisted conformer, which is interconverted with the *anti* conformer very fast at room temperature.

Optical and Electronic Properties. Both **1a** and **1e** formed yellow solutions in common organic solvents, emitting yellow fluorescence with similar fluorescence quantum yields (18.6 and 17.5%, respectively, as measured in CH_2Cl_2). In contrast, the orange solutions of **1b–d** in common organic solvents emitted weaker orange fluorescence with a lower fluorescence quantum yield (2% as measured in CH_2Cl_2) in relation to the presence of silylethynyl substituents. Since silylethynylated dibenzo[*a*,*m*]rubicenes **1b–d** exhibited almost identical UV–vis absorption and fluorescence spectra, Figure 3 only shows the absorption and fluorescence spectra of **1a**, **1b**, and **1e** in CH_2Cl_2 at the same concentration. It is found that

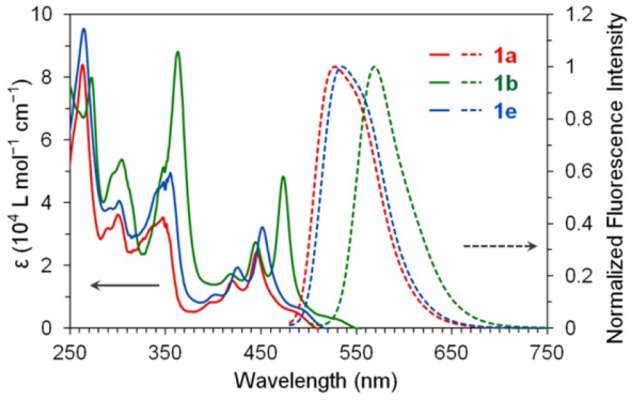

Figure 3. UV–vis absorption (solid lines) and fluorescence (dashed lines) spectra of **1a**, **1b**, and **1e** in solutions (5×10^{-6} M in CH_2Cl_2). The fluorescence spectra of **1a**, **1b**, and **1e** were recorded with excitation at 445, 473, and 451 nm, respectively.

DOI: 10.1021/jacs.5b10687
J. Am. Chem. Soc. 2015, 137, 16203–16208

Table 1. Absorption, Reduction Potentials, and Frontier Molecular Orbital Energy Levels of 1a−e

	experimental						calculated[f]					
							HOMO (eV)		LUMO (eV)		gap (eV)	
	λ_{max} (nm)[a]	λ_{edge} (nm)[a]	E_{red} (V)[b]	LUMO (eV)[c]	HOMO (eV)[d]	gap (eV)[e]	twisted	*anti*	twisted	*anti*	twisted	*anti*
1a	445	508	−1.80	−3.30	−5.74	2.44	−5.67	−5.69	−2.68	−2.67	2.99	3.02
1b	473	551	−1.57	−3.53	−5.78	2.25	−5.65	−5.66	−2.89	−2.88	2.76	2.78
1c	473	551	−1.56	−3.54	−5.79	2.25	−5.66	−5.66	−2.89	−2.89	2.77	2.77
1d	473	551	−1.57	−3.53	−5.78	2.25	−5.63	−5.63	−2.87	−2.86	2.76	2.77
1e	451	515	−1.83	−3.27	−5.68	2.41	−5.50	−5.51	−2.53	−2.53	2.97	2.98

[a]The wavelength of maximum absorption in the visible light region (λ_{max}) and the wavelength of absorption edge (λ_{edge}) from a 5×10^{-6} M solution in CH_2Cl_2. [b]Half-wave potential versus ferrocenium/ferrocene for the first reduction wave. [c]Estimated from LUMO = −5.10 − E_{red} (eV). [d]Calculated from the HOMO−LUMO gap and the LUMO energy level. [e]HOMO−LUMO gap estimated from λ_{edge}. [f]Calculated at the B3LYP level of DFT with 6-311++G(d,p)//6-31G(d,p) basis sets.

the absorption spectrum of **1b** is red-shifted by 28 nm relative to that of **1a**, as measured from the longest wavelength absorption maxima, while the absorption spectrum of **1e** exhibits a much smaller red shift relative to that of **1a**, likely because the substituting phenyl groups are almost orthogonal to the polycyclic backbone with poor conjugation. As shown in Figure 3, the fluorescence spectra of **1a**, **1b**, and **1e** exhibit Stokes shifts of 0.43, 0.44, and 0.38 eV, respectively. These large Stokes shifts are in agreement with the fact that **1a−e** are flexible molecules with a small energy barrier between the twisted and *anti* conformations.

The redox behaviors of **1a−e** in solution were investigated with cyclic voltammetry. In the test window of cyclic voltammetry, **1a−e** did not exhibit any oxidation waves. **1a−c** and **1e** all exhibited one quasi-reversible reduction wave, while **1d** exhibited two quasi-reversible reduction waves (Figure S1 in the Supporting Information). Based on the first reduction potential[15] as well as the absorption edges found from the UV−vis absorption spectra, the energy levels of the highest occupied molecular orbital (HOMO) and the lowest unoccupied molecular orbital (LUMO) for **1a−e** are estimated and summarized in Table 1. The frontier molecular orbitals of **1a−e** were also calculated with both the twisted and *anti* conformations. As summarized in Table 1, the twisted and *anti* conformers of each molecule have essentially the same HOMO and LUMO energy levels. As shown in the Supporting Information, the wave functions of HOMO and LUMO in **1a−e** are all delocalized over the entire π-backbone and essentially do not differ in the twisted and *anti* conformers. The calculated HOMO energy levels are in good agreement with the experimental values, while the calculated LUMO energy levels are higher than the corresponding experimental values by a larger degree similar to the reported CP-PAHs.[16] The calculated HOMO and LUMO energy levels of **1a** are both lower than the reported values of rubicene (−5.29 eV for HOMO and −2.54 eV for LUMO)[4] as a result of chromophore expansion by benzoannulation as well as deviation from planarity.

Crystal Structures. Single crystals of **1a** qualified for X-ray crystallography were grown by cooling its hot solution in toluene, and those of **1b−e** were grown from solutions in CH_2Cl_2−ethyl acetate by slow evaporation of solvents. As found from the crystal structures, the dibenzo[*a*,*m*]rubicene backbone of **1a−d** adopts a twisted conformation, while that of **1e** adopts an *anti* conformation in the crystals. With a twisted conformation, **1a** is a chiral molecule forming a racemic crystal. Figure 4a shows the *P*-enantiomer of **1a** having its fjord regions distorted with torsion angles of 13.9 and 16.2°. As shown in

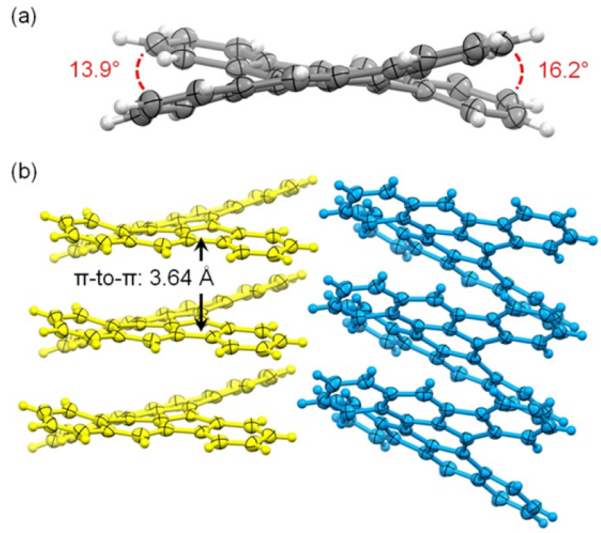

Figure 4. Crystal structure of **1a** showing (a) *P*-enantiomer and (b) $\pi-\pi$ stacking. C atoms are shown as ellipsoids at the 50% probability level. In (b), *M*-enantiomers are shown in yellow and the *P*-enantiomers in blue.

Figure 4b, the crystal of **1a** consists of segregated stacks of *M*- and *P*-enantiomers (shown in yellow and blue, respectively), and molecules of the same chirality stack with each other in one stack. Since the polycyclic backbone of **1a** can be regarded as two benzo[*b*]fluorene subunits joined by the central benzene ring, the π-to-π distance in a stack of **1a** can be determined by measuring the distance between the benzo[*b*]fluorene planes or the distance between the central benzene planes of two neighboring molecules. It is found that the stack of **1a** is associated with a π-to-π distance of 3.64 Å as measured from the distance between the two benzo[*b*]fluorene planes of neighboring molecules.

With essentially the same twisted backbone, **1b−d** also exist as a pair of enantiomers in racemic crystals. However, instead of forming segregated stacks, *M*- and *P*-enantiomers of **1b** form π-stacked columns with an alternate arrangement, as shown in Figure 5a. The π-to-π distance in this column is not measured because neither the central benzene rings nor the benzo[*b*]-fluorene planes in the neighboring molecules of **1b** are parallel with each other. Instead, intermolecular contacts shorter than double the van der Waals radius of carbon are found between carbon atoms in the alternate π-stack of **1b**, as also shown in Figure 5a. Moreover, this type of π-stacking involves a rotation of the *P*-enantiomer relative to the *M*-enantiomer below it, as

DOI: 10.1021/jacs.5b10687
J. Am. Chem. Soc. 2015, 137, 16203−16208

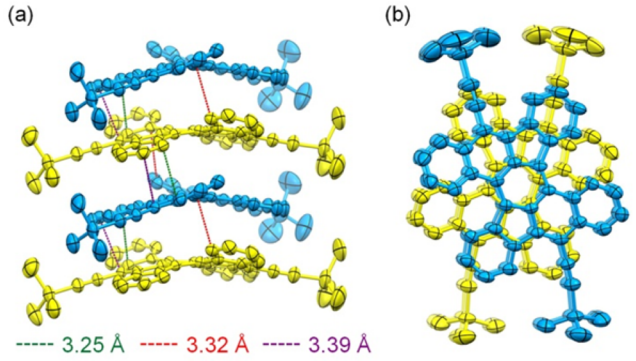

Figure 5. (a) Side view and (b) top view of the $\pi-\pi$ stacking of **1b** in the crystal. Hydrogen atoms are removed for clarification, and C and Si atoms are shown as ellipsoids at the 50% probability level. The *M*-enantiomers are shown in yellow and the *P*-enantiomers in blue.

shown in Figure 5b. With the trimethylsilyl group of **1b** replaced by a *t*-butyldimethylsilyl group, **1c** exhibits essentially the same molecular packing as **1b**, as found from its crystal structure. In contrast, further increasing the size of substituting groups leads to a very different molecular packing in the crystal structure of **1d** likely because the bulky triisopropylsilyl groups of **1d** cannot be accommodated in the columnar stacking of **1b** and **1c**. As shown in Figure 6, molecules of **1d** form shifted π-

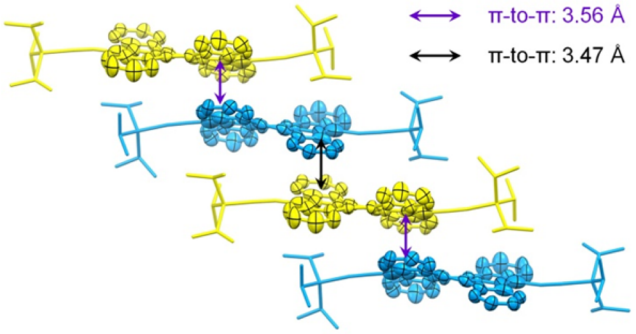

Figure 6. Crystal structure of **1d** showing $\pi-\pi$ stacking. Hydrogen atoms are removed for clarification. Carbon atoms in the polycyclic backbone are shown as ellipsoids at the 50% probability level, and silylethynyl substituents are shown as capped sticks. The *M*-enantiomers are shown in yellow and the *P*-enantiomers in blue.

stacks with an alternate arrangement of *M*- and *P*-enantiomers. The π-to-π distances between the adjacent *M*- and *P*-enantiomers of **1d** are 3.47 and 3.56 Å as measured from the distance between the two benzo[*b*]fluorene planes.

With a phenyl-substituting group, **1e** has an achiral *anti*-folded backbone of dibenzo[*a*,*m*]rubicene in the crystals. The torsion angle between the substituting phenyl group and the polycyclic backbone is about 80°. As twisted-**1e** dominates in the solution and converts to *anti*-**1e** fast, the presence of *anti*-**1e** in the crystals is likely a result from closer packing of *anti*-**1e** that accompanies lower solubility. The molecular packing of **1e** is dominated by an edge-to-face interaction between the substituting phenyl group and the polycyclic backbone, as shown in Figure 7. The distance between the hydrogen atom in the phenyl and the carbon atom in the polycyclic backbone is 2.67 Å, which is shorter than the sum of the van der Waals radii (2.79 Å). With such edge-to-face interaction, the adjacent

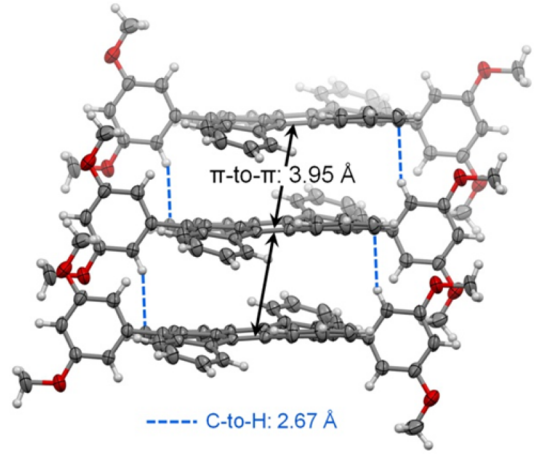

Figure 7. Molecular packing of **1e** in the single crystal. Carbon and oxygen atoms are shown as gray and red ellipsoids at the 50% probability level, and hydrogen atoms are shown as white balls.

molecules of **1e** are separated with a large distance of 3.95 Å between the central benzene rings of the polycyclic framework.

Semiconductor Properties. The HOMO energy levels and $\pi-\pi$ stacking of **1a–d** suggest that they can, in principle, function as p-type semiconductors. On the other hand, the large π-to-π distance of **1e** suggests an unfavorable molecular packing for organic semiconductors. To test the potential semiconductor properties of dibenzo[*a*,*m*]rubicenes in OTFTs, we first attempted to dip-coat thin films **1a–e** on a highly doped silicon substrate, which had a layer of SiO_2 on the surface as a dielectric. However, only **1b** and **1c** formed continuous films, while **1a**, **1d**, and **1e** formed isolated crystalline or amorphous domains on SiO_2. It was found that the dip-coated films of **1b** and **1c** on SiO_2 functioned as p-type semiconductors, exhibiting a field effect mobility of up to 1×10^{-3} and 2×10^{-4} $cm^2\ V^{-1}\ s^{-1}$, respectively. To improve the quality of organic films, we replaced the conventional SiO_2 with a high-*k* dielectric layer of AlO_y/TiO_x,[17] which was modified with a self-assembled monolayer (SAM) of 12-cyclohexyldodecylphosphonic acid (CDPA) to provide a dielectric surface with high molecular ordering and good wettability by common organic solvents.[18] As shown in Figure 8a, thin films of **1b** consisting of aligned crystalline fibers were formed by immersing the $CDPA/AlO_y/TiO_x$ substrate into a solution of **1b** (2 mg mL^{-1}) in 1:1 (v/v) CH_2Cl_2–acetone and then pulling it up with a constant speed of 1.3 $\mu m\ s^{-1}$. Under the

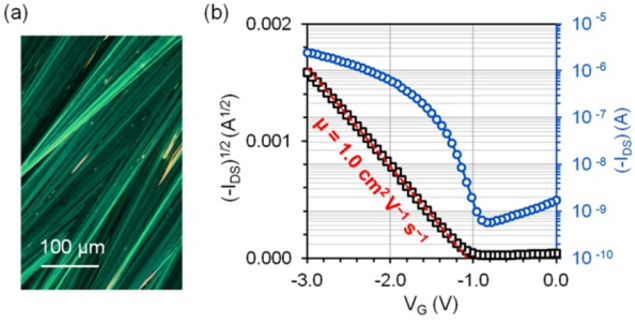

Figure 8. (a) Reflection polarized light micrograph for a dip-coated film of **1b**; (b) drain current (I_{DS}) versus gate voltage (V_{GS}) with drain voltage (V_{DS}) at −3 V for the best-performing OTFT of **1b** with an active channel of W = 1 mm and L = 150 μm measured in air.

DOI: 10.1021/jacs.5b10687
J. Am. Chem. Soc. 2015, 137, 16203–16208

same condition, except a higher pulling speed (5.0 μm s^{-1}), **1c** formed high-quality thin films with similar morphology, as shown in Figure S2 in the Supporting Information. In contrast, on the CDPA/AlO_y/TiO_x dielectric, **1a**, **1d**, and **1e** still could not form continuous films suitable for OTFTs, although varied concentrations and pulling speeds were tested. Instead, **1a** formed poorly connected needle-shaped crystallites, while **1d** and **1e** formed discrete amorphous domains, likely in relation to their molecular packing. The fabrication of OTFTs was completed by depositing a layer of gold on the film of **1b** or **1c** through a shadow mask to form top-contact source and drain electrodes. As measured in ambient air from at least 20 channels for each compound, **1b** and **1c** both functioned as p-type semiconductors with a field effect mobility of 0.8 ± 0.2 and 0.2 ± 0.1 cm^2 V^{-1} s^{-1}, respectively. The highest mobility of **1b** is 1.0 cm^2 V^{-1} s^{-1} as extracted from the transfer $I-V$ curve shown in Figure 8b, using the equation

$$I_{DS} = (\mu W C_i/2L)(V_{GS} - V_{th})^2$$

where I_{DS} is the drain current, μ is field effect mobility, C_i is the capacitance per unit area (210 nF cm^{-2}) for the CDPA/AlO_y/TiO_x dielectric, W is the channel width, L is the channel length, and V_{GS} and V_{th} are the gate and threshold voltage, respectively. In comparison to **1b**, 6,13-bis((triisopropylsilyl)ethynyl)-pentacene, a benchmark p-type semiconductor, in solution-processed transistors on the same CDPA/AlO_y/TiO_x dielectric exhibited a higher field effect mobility (1.64 ± 0.55 cm^2 V^{-1} s^{-1}),[18] while rubicene in vacuum-deposited bottom-contact OTFTs on bare SiO_2 exhibited a lower mobility (0.32 ± 0.04 cm^2 V^{-1} s^{-1}).[4]

To better understand the measured field effect mobilities of **1b** and **1c** in relation to their assemblies in the solid state, their thin films were investigated with UV−vis absorption spectroscopy, X-ray diffraction (XRD), and atomic force microscopy (AFM). The dip-coated film of **1b** on a quartz plate, similar to that of **1c**, exhibited a broadened and red-shifted absorption spectrum relative to that of the solution, as shown in Figure S5 in the Supporting Information. This can be attributed to electronic delocalization between π-stacked molecules in the solid state, in agreement with the crystal structures.[19,20] X-ray diffraction patterns from the films of **1b** on CDPA/AlO_y/TiO_x (Figure S6 in the Supporting Information) exhibited peaks at 2θ = 4.51 (d spacing of 19.6 Å), 2θ = 18.09 (d spacing of 4.9 Å), and 2θ = 22.66 (d spacing of 3.9 Å). These peaks correspond to the (010), (040), and (050) diffractions as derived from the single-crystal structure of **1b**, indicating a highly ordered film with the b axis perpendicular to the substrate surface. The AFM image for the film of **1b** (Figure S10 in the Supporting Information) revealed a smooth surface containing highly ordered flat microstripes of ca. 1 μm wide. Section analysis revealed a molecular step of ca. 1.9 nm high, which is in agreement with the d spacing of 19.6 Å and the molecular length of **1b** (19.5 Å) as measured between the two trimethylsilyl groups from the crystal structure. The XRD and AFM indicate that molecules of **1b** adopt an edge-on orientation on the surface of the CDPA/AlO_y/TiO_x dielectric and have their π-backbones stacked in a column roughly parallel to the surface. X-ray diffraction patterns from the films of **1c** on CDPA/AlO_y/TiO_x (Figure S7 in the Supporting Information) exhibited peaks at 2θ = 5.48 (d spacing of 16.1 Å), 2θ = 16.48 (d spacing of 5.4 Å), and 2θ = 27.63 (d spacing of 3.2 Å). These peaks correspond to (110), (330), and (550) diffractions as derived from the single-crystal structure of **1c**, indicating a highly ordered film with the (110) plane parallel to the substrate surface. As found from the AFM image (Figure S10 in the Supporting Information), the film of **1c** consisted of similar microstripes of ca. 1 μm wide but were rougher than that of **1b**. Section analysis revealed a molecular step of ca. 1.6 nm high, which is in agreement with the d spacing of 16.1 Å. The XRD and AFM indicate that molecules of **1c** stand on the surface of the CDPA/AlO_y/TiO_x dielectric with an orientation slightly different than that of **1b** but still stack in a column roughly parallel to the surface, as shown in Figure S12 in the Supporting Information. The AFM section analysis on the film of **1c** also shows deeper grain boundaries, which may account for the lower mobility of **1c** in thin films. In comparison to the films on CDPA/AlO_y/TiO_x, the dip-coated film of **1b** on bare SiO_2 exhibited the (200) and (400) diffractions in addition to the (010), (040), and (050) diffractions, while the dip-coated film of **1c** on bare SiO_2 exhibited the (020) and (040) diffractions in addition to the (110), (330), and (550) diffractions. The existence of an extra set of diffraction peaks indicates that molecules of **1b** are not uniformly oriented in the film on bare SiO_2, and neither do those of **1c**. In comparison to the films on CDPA/AlO_y/TiO_x, the dip-coated films of **1b** and **1c** on bare SiO_2 contained much rougher microstripes that accompany much deeper grain boundaries, as found from their AFM images (Figure S11 in the Supporting Information). Therefore, the much lower mobility for the films of **1b** and **1c** on bare SiO_2 can be explained as a result of poorer crystallinity and morphology.

CONCLUSION

In conclusion, the above study puts forth a new class of polycyclic arenes containing fused five-membered rings. We have developed an efficient synthesis of dibenzo[a,m]rubicene and its derivatives and demonstrated that the conformation and molecular packing of dibenzo[a,m]rubicenes in the solid state are dependent on the substituting groups. With a nonplanar conjugated backbone, **1b** and **1c** function as p-type organic semiconductors in solution-processed OTFTs exhibiting a field effect mobility of up to 1.0 cm^2 V^{-1} s^{-1}, which is higher than those of the reported semiconductors based on CP-PAHs.[4,21] This finding, together with a few reports on organic semiconductors with nonplanar polycyclic conjugated backbones,[22−25] suggests that a planar π-backbone is not the only choice for designing high-mobility organic semiconductors.

ASSOCIATED CONTENT

Supporting Information

The Supporting Information is available free of charge on the ACS Publications website at DOI: 10.1021/jacs.5b10687.

Experimental details of synthesis and characterization, fabrication and characterization of organic thin film transistors, and NMR spectra (PDF)
Crystallographic information files for **1a** (CIF)
Crystallographic information files for **1b** (CIF)
Crystallographic information files for **1c** (CIF)
Crystallographic information files for **1d** (CIF)
Crystallographic information files for **1e** (CIF)

AUTHOR INFORMATION

Corresponding Author

*miaoqian@cuhk.edu.hk

DOI: 10.1021/jacs.5b10687
J. Am. Chem. Soc. 2015, 137, 16203−16208

Notes

The authors declare no competing financial interest.

■ ACKNOWLEDGMENTS

We thank Ms. Hoi Shan Chan (The Chinese University of Hong Kong) for the single-crystal crystallography. This work was supported by the Research Grants Council of Hong Kong (CRF C4030-14G) and the Chinese University of Hong Kong (the Faculty Strategic Development Scheme from the Faculty of Science and the One-Off Funding for Research from Research Committee).

■ REFERENCES

(1) For recent examples of CP-PAHs, see: (a) Chase, D. T.; Rose, B. D.; McClintock, S. P.; Zakharov, L. N.; Haley, M. M. *Angew. Chem., Int. Ed.* **2011**, *50*, 1127−1130. (b) Chase, D. T.; Fix, A. G.; Rose, B. D.; Weber, C. D.; Nobusue, S.; Stockwell, C. E.; Zakharov, L. N.; Lonergan, M. C.; Haley, M. M. *Angew. Chem., Int. Ed.* **2011**, *50*, 11103−11106. (c) Shimizu, A.; Tobe, Y. *Angew. Chem., Int. Ed.* **2011**, *50*, 6906−6910. (d) Zhang, Q.; Kawasumi, K.; Segawa, Y.; Itami, K.; Scott, L. T. *J. Am. Chem. Soc.* **2012**, *134*, 15664−15667. (e) London, G.; von Wantoch Rekowski, M.; Dumele, O.; Schweizer, W. B.; Gisselbrecht, J.-P.; Boudon, C.; Diederich, F. *Chem. Sci.* **2014**, *5*, 965−972. (f) Liu, E.-C.; Chen, M.-K.; Li, J.-Y.; Wu, Y. T. *Chem. - Eur. J.* **2015**, *21*, 4755−4761. (g) Sbargoud, K.; Mamada, M.; Marrot, J.; Tokito, S.; Yassar, A.; Frigoli, M. *Chem. Sci.* **2015**, *6*, 3402−3409. (h) Nobusue, S.; Miyoshi, H.; Shimizu, A.; Hisaki, I.; Fukuda, K.; Nakano, M.; Tobe, Y. *Angew. Chem., Int. Ed.* **2015**, *54*, 2090−2094. (i) Dutta, A. K.; Linden, A.; Zoppi, L.; Baldridge, K. K.; Siegel, J. S. *Angew. Chem., Int. Ed.* **2015**, *54*, 10792−10796.

(2) Hseuh, H.-H.; Hsu, M.-Y.; Wu, T.-L.; Liu, R.-S. *J. Org. Chem.* **2009**, *74*, 8448−8451.

(3) (a) Pummerer, R.; Ulrich, H. M. *Ber. Dtsch. Chem. Ges.* **1925**, *58*, 1806−1808. (b) Schlenk, W.; Karplus, M. *Ber. Dtsch. Chem. Ges.* **1928**, *61*, 1675−1680.

(4) Lee, H.; Zhang, Y.; Zhang, L.; Mirabito, T.; Burnett, E. K.; Trahan, S.; Mohebbi, A. R.; Mannsfeld, S. C. B.; Wudl, F.; Briseno, A. L. *J. Mater. Chem. C* **2014**, *2*, 3361−3366.

(5) Dithiarubicene, which has two benzene rings in rubicene replaced by two thiophene rings, was also recently reported. See: Mohebbi, A. R.; Wudl, F. *Chem. - Eur. J.* **2011**, *17*, 2642−2646.

(6) For recent examples of double helicenes, see: (a) Fujikawa, T.; Segawa, Y.; Itami, K. *J. Am. Chem. Soc.* **2015**, *137*, 7763−7768. (b) Kashihara, H.; Asada, T.; Kamikawa, K. *Chem. - Eur. J.* **2015**, *21*, 6523−6527. (c) Lütke Eversloh, C.; Liu, Z.; Müller, B.; Stangl, M.; Li, C.; Müllen, K. *Org. Lett.* **2011**, *13*, 5528−5531.

(7) Dougherty, K. J.; Kraml, C. M.; Byrne, N.; Porras, J. A.; Bernhard, S.; Mague, J. T.; Pascal, R. A., Jr *Tetrahedron* **2015**, *71*, 1694−1699.

(8) White, D. M. *J. Org. Chem.* **1974**, *39*, 1951−1952.

(9) Merlet, S.; Birau, M.; Wang, Z. Y. *Org. Lett.* **2002**, *4*, 2157−2159.

(10) For examples of synthesis of polycylic arenes using the Corey−Fuchs reaction with similar conditions, see: (a) Donovan, P. M.; Scott, L. T. *J. Am. Chem. Soc.* **2004**, *126*, 3108−3112. (b) Loo, Y.-L.; Hiszpanski, A. M.; Kim, B.; Wei, S.; Chiu, C.-Y.; Steigerwald, M. L.; Nuckolls, C. *Org. Lett.* **2010**, *12*, 4840−4843. (c) Cheung, K. Y.; Xu, X.; Miao, Q. *J. Am. Chem. Soc.* **2015**, *137*, 3910−3914.

(11) (a) Anthony, J. E.; Brooks, J. S.; Eaton, D. L.; Parkin, S. R. *J. Am. Chem. Soc.* **2001**, *123*, 9482−9483. (b) Anthony, J. E.; Eaton, D. L.; Parkin, S. R. *Org. Lett.* **2002**, *4*, 15−18.

(12) Luo, J.; Xu, X.; Mao, R.; Miao, Q. *J. Am. Chem. Soc.* **2012**, *134*, 13796−13803.

(13) (a) Becke, A. D. *J. Chem. Phys.* **1993**, *98*, 5648−5652. (b) Miehlich, B.; Savin, A.; Stoll, H.; Preuss, H. *Chem. Phys. Lett.* **1989**, *157*, 200−206. (c) Lee, C.; Yang, W.; Parr, R. G. *Phys. Rev. B: Condens. Matter Mater. Phys.* **1988**, *37*, 785−789.

(14) Anslyn, E. V.; Dougherty, D. A. *Modern Physical Organic Chemistry*; University Science Books: Sausalito, CA, 2004; Chapter 7.

(15) The commonly used formal potential of the redox couple of ferrocenium/ferrocene (Fc^+/Fc) in the Fermi scale is −5.1 eV, which is calculated on the basis of an approximation neglecting solvent effects using a work function of 4.46 eV for the normal hydrogen electrode (NHE) and an electrochemical potential of 0.64 V for Fc^+/Fc versus NHE. See: Cardona, C. M.; Li, W.; Kaifer, A. E.; Stockdale, D.; Bazan, G. C. *Adv. Mater.* **2011**, *23*, 2367−2371.

(16) (a) Wood, J. d.; Jellison, K. L.; Finke, A. D.; Wang, L.; Plunkett, K. N. *J. Am. Chem. Soc.* **2012**, *134*, 15783−15789. (b) Chaolumen; Murata, M.; Sugano, Y.; Wakamiya, A.; Murata, Y. *Angew. Chem., Int. Ed.* **2015**, *54*, 9308−9312.

(17) Su, Y.; Wang, C.; Xie, W.; Xie, F.; Chen, J.; Zhao, N.; Xu, J. *ACS Appl. Mater. Interfaces* **2011**, *3*, 4662−4667.

(18) Liu, D.; He, Z.; Su, Y.; Diao, Y.; Mannsfeld, S. C. B.; Bao, Z.; Xu, J.; Miao, Q. *Adv. Mater.* **2014**, *26*, 7190−7196.

(19) Miao, Q.; Chi, X.; Xiao, S.; Zeis, R.; Lefenfeld, M.; Steigerwald, M. L.; Siegrist, T.; Nuckolls, C. *J. Am. Chem. Soc.* **2006**, *128*, 1340−1345.

(20) Lim, S.-H.; Bjorklund, T. G.; Spano, F. C.; Bardeen, J. C. *Phys. Rev. Lett.* **2004**, *92*, 107402.

(21) (a) Kawase, T.; Fujiwara, T.; Kitamura, C.; Konishi, A.; Hirao, Y.; Matsumoto, K.; Kurata, H.; Kubo, T.; Shinamura, S.; Mori, H.; Miyazaki, E.; Takimiya, K. *Angew. Chem., Int. Ed.* **2010**, *49*, 7728−7732. (b) Chase, D. T.; Fix, A. G.; Kang, S. J.; Rose, B. D.; Weber, C. D.; Zhong, Y.; Zakharov, L. N.; Lonergan, M. C.; Nuckolls, C.; Haley, M. M. *J. Am. Chem. Soc.* **2012**, *134*, 10349−10352. (c) Nishida, J.-i.; Tsukaguchi, S.; Yamashita, Y. *Chem. - Eur. J.* **2012**, *18*, 8964−8970. (d) Xia, H.; Liu, D.; Xu, X.; Miao, Q. *Chem. Commun.* **2013**, *49*, 4301−4303.

(22) Ball, M.; Zhong, Y.; Wu, Y.; Schenck, C.; Ng, F.; Steigerwald, M.; Xiao, S.; Nuckolls, C. *Acc. Chem. Res.* **2015**, *48*, 267−276.

(23) Xiao, S.; Myers, M.; Miao, Q.; Sanaur, S.; Pang, K.; Steigerwald, M. L.; Nuckolls, C. *Angew. Chem., Int. Ed.* **2005**, *44*, 7390−7394.

(24) Gsänger, M.; Oh, J. H.; Könemann, M.; Höffken, H. W.; Krause, A.-M.; Bao, Z.; Würthner, F. *Angew. Chem., Int. Ed.* **2010**, *49*, 740−743.

(25) Shan, L.; Liu, D.; Li, H.; Xu, X.; Shan, B.; Xu, J.-B.; Miao, Q. *Adv. Mater.* **2015**, *27*, 3418−3423.

DOI: 10.1021/jacs.5b10687
J. Am. Chem. Soc. 2015, 137, 16203−16208